# Characterization of candidate stellar merger progenitors

Author: Hui Hui Zhang Guo, hzhanggu7@alumnes.ub.edu Facultat de Física, Universitat de Barcelona, Diagonal 645, 08028 Barcelona, Spain.

Advisor: Nadejda Blagorodnova, nblago@fqa.ub.edu

**Abstract:** Stellar mergers have traditionally been detected because of their outbursts. A study by Addison et al.(2022) proposed a method to select them based on their position in the Hertzsprung Gap and an increase in luminosity, although without extinction values, resulting in 21 progenitor candidates for Luminous Red Novae. We present their characterization study based on new photometric and spectroscopic data. Initially identified as yellow stars, all candidates were found to be B-type stars, most of them Be stars, which makes them unlikely to be genuine LRNe progenitors. These results underscore the need to incorporate extinction corrections to avoid mischaracterization due to reddening effects. We also compute variation in radial velocities in order to decide if they may be binary systems and rotation velocities for the sources without emission lines, since Be stars are usually fast rotators. As expected, their rotational velocity to critical velocity ratio is 0.47-0.64. **Keywords:** Astrophysics, Observational Astronomy, Atomic transitions.

SDGs: Quality education, Gender equality.

#### I. INTRODUCTION

Binary stellar systems are not uncommon in our Universe. Conversely, a great fraction of stars are born as binary or multiple systems, and the fraction increases among massive stars, rising to 70% of them [19]. As summarized in [4], their relevance lies in the interactions between the stars, which can alter their structure and evolution and lead to the formation of objects whose existence cannot be explained by standard single star evolution models. Also, they can provide a different way to determine stellar masses, radius, and luminosities.

If the separation between the system's stars is small enough, they may end up merging. If the primary donor is on its fast expansion, there is a possibility of starting an unstable mass transfer to its companion. Hydrostatic equilibrium can not be maintained, causing a mass runaway and the formation of a non-corotating gaseous layer where both stars orbit: the common envelope (CE). Studies suggests that this usually happens in the Hertzsprung Gap (HG), when stars evolve off the Main Sequence (MS) towards the Red Giant Branch (RGB), becoming a Yellow Giant (YG) or a Yellow Super Giant (YSG). This stage of a star's life is short, lasting only about a thousand years, depending on its initial mass. Yet, the radius can increase by nearly an order of magnitude. At some point, the less massive star spirals into the gravitational well of the massive star, transferring the angular momentum of the binary to the envelope. Eventually, the CE is ejected as a Luminous Red Nova (LRN), an astrophysical transient with a peak brightness located between that of novae and supernovae.

Up until now, binary systems have never been studied prior to their merger, but always during their outburst. However, it is in our interest to predict mergers. Being able to identify LRN ahead of time using its progenitor's characteristics would shed light into the mass transfer mechanism processed in the binary star just a few years before its merger.

Before the main outburst, outflows from the pre-CE phase have shown to produce a rise in luminosity of a few magnitudes 2-10 years prior the ejection. A previous paper [1] presented a method to identify LNR candidates from evolved HG stars that presented variability by studying their time-domain light curves and looking for this increase. The result was a selection of 21 candidates likely to outburst within the next 1-10 years, nearly all of which presented Hydrogen emission lines in their low-resolution spectra. These spectroscopic observations showed that they may be mass-transferring binaries surrounded by dusty interstellar discs or magnetically active stellar merger remnants. However, the limitations of the spectroscopic resolution did not allow a careful study of narrow lines and spectral features. The purpose of this research is to provide a more accurate characterization of all 21 sources using newly acquired high-resolution, multi-epoch spectroscopic data from the NOT/FIES spectrograph. The aim of this project is to identify the true candidates and rule out the contaminants among them, as well as determining the reason they have been identified as LRN progenitors by determining their spectral types and the origin of their variability.

### II. DATASETS

**Photometry** Since the base article for this current work was published in September 2022, there are more than two years of new photometric data. The sources from the last study of [1] were selected based on an increase in the luminosity of HG stars; their light curves were collected again to see the time evolution in the last two years and if there has been a LRN outburst since then. Data was taken from the Zwicky Transient Facility (ZTF) [2] time-domain survey using the Python package ztfquery. Searches were made in a radius of two arc seconds around the sources, collecting g, r and i band data. It was revised so that data points with

flagged problematic values were removed, since it ensures the quality of the photometry. Sources with high *chi* or *sharp* values were also eliminated. The former indicate poor fit quality between the source's profile and the Point-Spread Function (PSF), which describes the intensity distribution of a point source; while the latter reflects a deviation from a point-source shape.

**Spectroscopy** Spectra were obtained with the high-resolution FIbre-fed Echelle Spectrograph (FIES) at the Nordic Optical Telescope (NOT), which includes a reduction software for data analysis. Data reduction and calibration were performed using the instrument's pipeline and [23, Gaia DR3]'s low resolution spectra. The data were taken in two separate nights—on November 12, 2023 and November 02—in order to detect binary companions. The low-resolution fibre was used, which covers a wavelength range of 3630-9270 Å and has a resolution of R=25000, since this fibre suffers the least from seeing losses and losses due to atmospheric dispersion. The system's efficiency is low for very blue wavelengths and for infrared, so perturbations can be seen at those ranges.

Figure 1 shows the light curve and spectrum of one of the 21 sources; the remaining ones can be found in the Appendix. The notation to identify the sources will be YSG\_RA\_Dec as in [1], with RA and Dec their integer coordinates in degrees.

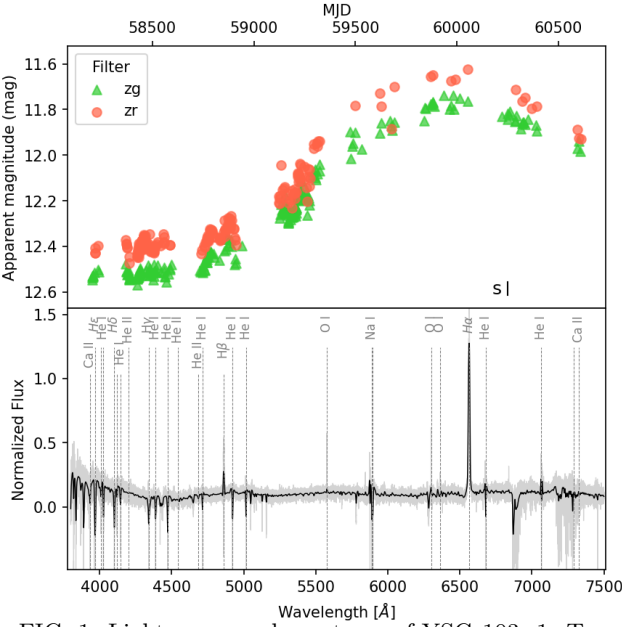


FIG. 1: Light curve and spectrum of YSG\_103\_-1. Top: apparent magnitude over time in MJD under two different filters. The symbol "|" shows the epoch in which the spectrum displayed in the lower panel was obtained. Bottom: flux as a function of wavelength, with the identification of the most important emission or absorption lines for stars with different temperatures. A Gaussian smoothing with  $\sigma=81\,\text{Å}$  and a polynomial fit were performed to remove the source's broad continuum. The fitting procedure involved a heavy smoothing step of  $\sigma=1627\,\text{Å}$  to get the general shape, the fitting of a third degree polynomial, and then the division of the original spectrum by the polynomial fit.

### III. ANALYSIS

This section presents the methodology implemented to analyse the available data.

#### A. Spectral classification

The most prominent emission and absorption lines in the spectrum of each source have been identified, as well as telluric absorption from the atmosphere. Those lines can be used to identify the spectral type of the sources making use of [10], a spectral classification atlas, which classifies them in the MK system. In addition, the presence of prominent emission lines allow us to classify them according to the criteria established in [11].

## B. Color Magnitude Diagram

The next step consisted in locating the sources in a colour magnitude diagram (CMD), in order to compare the old position, based on values taken from [5, Gaia DR2] and [6, Gaia EDR3], which did not account for extinction, with present data, where de-reddened values were obtained from [12, SHBoost], a catalogue of stellar properties derived from Gaia DR3 XP (RP/BP) spectra, astrometry and multi-wavelength photometry. This implies that absolute magnitudes are now extinction-corrected. To visualize their position in the CMD, a random sample with good parallaxes of 3895 stars has been collected from Gaia DR3. A parallax over error higher than 20 has been the criteria to select the stars with the most accurate distances.

Even though updated magnitude values are provided by SHBoost, extinction can also be estimated from our high-resolution spectroscopy. The applied method is provided by [8], which measures extinction using Diffuse Interstellar Bands (DIBs). The equivalent widths of 5780 Å and 6614 Å DIBs were measured, since there exists a correlation between these and the column density of interstellar material, and therefore the line-of-sight extinction.

Firstly, as recommended by the article, a smoothing process of  $\sigma = 16 \,\text{Å}$  was performed to decide the limits where the equivalent width would be computed, although the function equivalent\_width() of specutils must be called upon the original spectra. The spectrum is normalized to a continuum level of 1 making use of the function fit\_generic\_continuum() on an interval around the DIB's wavelength. Since the sources presented a very limited number of absorption lines, contamination from the stellar photosphere could be neglected, according to the same article. Once equivalent width values were obtained, E(B-V) were computed using equations (4) and (5) of [8]. Then, E(B-V) values were transformed into  $A_V$  values. For this purpose, a total-to-selective reddening law  $R_V$  of 3.1 was assumed, since it is the most commonly used for Milky Way dust. The general relation adopted in astronomy is  $A_V = R_V \cdot E(B - V)$ . Since two different values of visible-band extinction were obtained from two DIBs, a weighted average was computed to get a single value. At this point, we needed to transform the extinction in visual to the Gaia's DR3 photometric system. To accomplish this, we used the Python package extinction, with the Gaia filter effective wavelengths given by the SVO Filter Profile Service [18]. Absolute magnitude and apparent magnitude are related by  $M_X = m_X - 5\log_{10}(d) + 5 - A_X$ , for each band X.

### C. Radial Velocity

Since spectroscopic data from two epochs separated by 10 days were available, a cross-correlation function (CCF) was applied to detect variations in the radial velocity (RV) of the sources. The aim would be to detect a shift in RV induced by the orbital motion in a binary star system. However, multiple epochs would be needed to secure such detections reliably.

Cross-correlation analysis is a technique that can measure the similarity between two lines, revealing how one is related with another when shifted by a specific amount. The CCF is computed for different lags, presenting a maximum for a lag that matches both lines. In this work, it was implemented on He I 4388 Å, 4922 Å and 5016 Å absorption lines because of their photospheric origin and their stability. To ensure that the code worked, an artificial Doppler shift was added to the line to test if the shift could be recovered by this method. The shift is related with velocity by the expression  $v_r = \frac{\Delta \lambda}{\lambda_0} \cdot c$ , where c is the velocity of light in vacuum and  $\lambda_0$  the rest-wavelength of the lines.

### D. Rotation velocity

Further analysis was performed on the sources that did not present any emission lines. Rotation velocity was computed for each star based on the Full Width at Half Maximum (FWHM) of He I 4471 Å absorption line. The selection stems from its photospheric origin, so that it is not contaminated by disk emission and the fact that it is a common line used for Be-star's rotation velocities, as stated in [21]. For this purpose, a Gaussian profile was fitted to the spectral line to compute its FWHM. The rotation velocity is derived from the following expression, provided by [7], where i is the inclination of the source, which can approximately be inferred from the line profile:

$$v_{rot} \sin i = c \cdot \frac{FWHM}{2\lambda \cdot (\ln 2)^{1/2}} \tag{1}$$

## IV. RESULTS

Although there is a lack of data for some epochs, the available photometric data shows no significant increase in apparent magnitude since 2022. The sources exhibited a 0.2-0.8 magnitude increase in luminosity for 1–4 years, with some reverting to earlier luminosity levels and others stabilizing at a higher level.

Most of the sources are peculiar in the sense that they present numerous emission lines. The most important spectroscopic features are displayed in Table I. Among them, 17 are H $\alpha$  emitters, with some of them also presenting H $\beta$ , Fe II, He I, Na I or Ca II lines, the latter two of which are of interstellar origin.

Source	$H\alpha$	$H\beta$	FeII	Не і	Сан НК	CaT
YSG_3_60	P1	E+A	P1	PC	A	E
$YSG_3_62$	L1	E+A	L1	-	A	$\mathbf{E}$
$YSG_7_63$	P1	$\mathbf{E}$	P1	PC	A	$\mathbf{E}$
$YSG_14_60$	H1	E+A	H1	A	A	$\mathbf{E}$
$YSG_27_63$	A	A	-	A	A	-
$YSG_28_55$	P1	E+A	P1	PC	A	$\mathbf{E}$
$YSG\_30\_62$	A	A	-	A	A	-
$YSG_34_57$	E+A	E+A	A	A	A	A
$YSG_34_64$	$\mathbf{E}$	A	-	A	A	-
$YSG_39_57$	P1	E+A	P1	PC	A	$\mathbf{E}$
$YSG_{-}66_{-}44$	P1	$\mathbf{E}$	P1	PC	A	$\mathbf{E}$
$YSG_87_28$	E1	E+A	E1	A	A	A
$YSG_88_20$	L1	E+A	L1	PC	A	$\mathbf{E}$
$YSG_95_6$	E+A	A	-	A	A	-
YSG_1031	E+A	E+A	-	${\rm IPC}$	$A_{TP}$	${\rm IPC}$
YSG_10413	E+A	E+A	-	A	A	-
YSG_11021	$\mathbf{E}$	E+A	-	A	A	$\mathbf{E}$
$YSG\_298\_42$	E+A	E+A	-	A	A	-
YSG_316_47	E+A	E+A	L1	A	A	-
YSG_358_63	A	A	-	A	A	-
YSG_359_63	A	A	-	A	A	-

TABLE I: Spectral features of the sources, where E stands for emission and A for absorption. P, L, H, E indicates the profile code, where 1 or 2 means symmetrical or asymmetrical, respectively. (I)PC indicates a (inverse) P-Cygni profile. TP is short for triple peak.

It has been observed that none of the 21 sources of our sample can be an O-type star since they do not present He II 4200 Å or 4542 Å absorption lines, exclusive for this type of very hot stars. They can't be A type stars either, since we have not identified low-ionization lines, such as Mn I, Ca I, Fe I absorption lines. Moreover, the presence of the HeI absorption line and the absence of the HeII absorption line indicate that they are most likely B-type stars. Figure 2 shows the most notorious emission and absorption lines of YSG<sub>-</sub>7<sub>-</sub>63, where a sigma-clipping has been performed to substitute data points further than two sigmas away from the median average value, caused by photons of cosmic rays during the observation. Therefore, the sources are high temperature blue stars, opposed to the original categorization of them as YSG in the HG due to the lack of extinction values.

Be stars Evidence shows that all 21 sources are B-type stars, most of which exhibit emission lines and therefore can be classified as a special type of Btype stars: Be stars. Although YSG\_27\_63, YSG\_30\_62, YSG\_358\_63 and YSG\_359\_63 do not show emission lines, they are fast-rotating B-type stars, which is also consistent with Be star characteristics. Be stars are emission line stars that are characterized by emission in the Balmer, Paschen, Brackett and other Hydrogen lines, sometimes accompanied by emission of singly ionized metals, most commonly Fe II, which is a key ion to classify this kind of stars. Observations indicate that Be stars are rapidly rotating main sequence stars that are surrounded by a Keplerian disk in its equatorial plane. According to [14], the high rotational velocity leads to mass ejection,

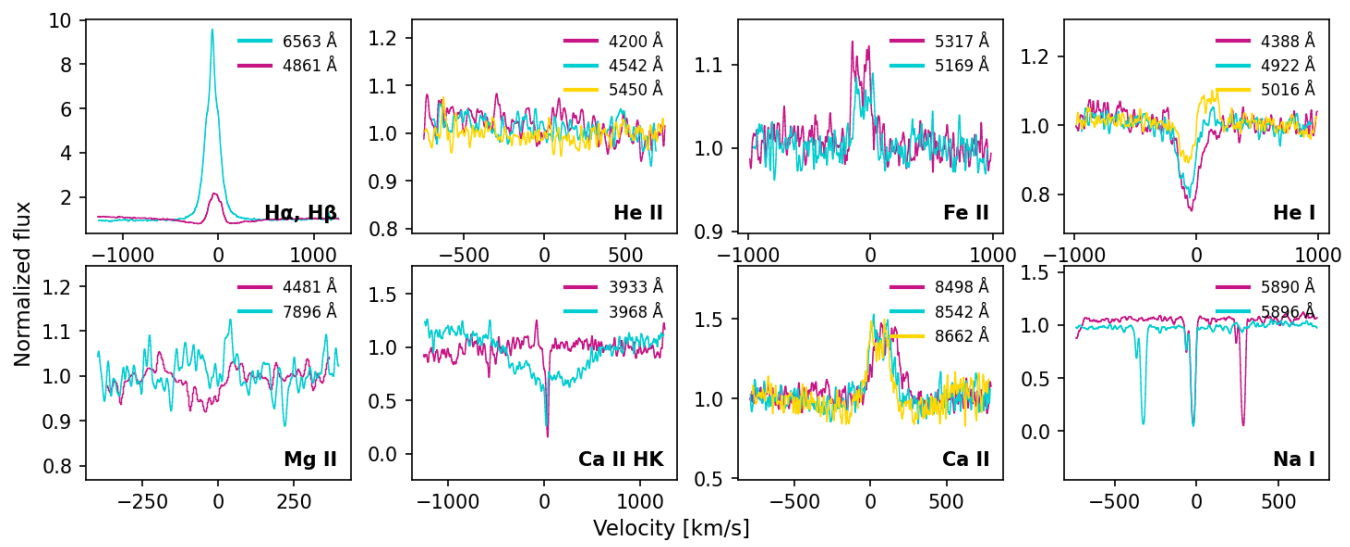


FIG. 2: Emission and absorption lines of YSG\_7\_63 as normalized flux in function of velocity (km/s). The spectrum has been continuum-normalized dividing the flux by the mean level computed from regions adjacent to the line, excluding the line core.

resulting in the formation of the disk. The emission lines are thought to arise from the hot circumstellar gas in this disk, with shell (narrow absorption) lines appearing when the disk is seen edge-on. As a fact, spectral and photometric variability are key features of Be stars. Moreover, the fact that the sources are Be stars would also explain the outburst seen in their light curves, which led to their selection as LRN progenitor candidates. As affirmed by [13], disk formation in Be stars leaves its imprint in the light curve, consistent with the observed behaviour.

Be stars' emission spectrum can be grouped based on the profiles of H $\alpha$  and Fe II lines, according to the classification system provided by [11]. Their system uses three main parameters: the disk's kinematics decide if the profile is symmetric (class 1) or asymmetric (class 2); optical depth of the gas, being H $\alpha$  at 6563 Å an optically thick emission line and Fe II at 5317 Å the optically thin emission line; and inclination of the circumstellar disk. Figure 3 shows how the profile varies with inclination for symmetrical profiles, going from a point of view above the circumstellar disc to its side.

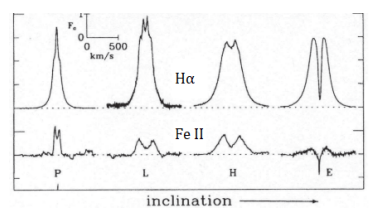


FIG. 3: Typical emission-line shapes for symmetrical H $\alpha$  and Fe II profiles in [11]'s system.

The narrow absorption line in the core indicates a shell profile, origined by absorption in the disk, becoming a B-type shell star. The article [11] provides a classification diagram that has been applied, as shown in Figure 4. The results of the categorization by the previously mentioned criteria are displayed in Table I.

It is worth mentioning the P Cygni profile of some He I lines, a spectroscopic feature which indicates the ex-

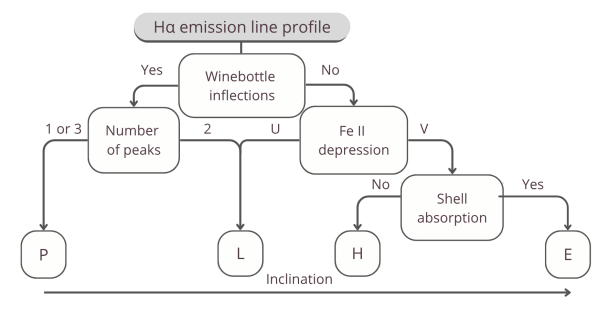


FIG. 4: Line-profile classification scheme of Be stars based on criteria from [11].

istence of a gaseous envelope expanding away from the star, caused by stellar winds. It appears as both an absorption and emission in the profile of the same line. The emission line arises from a dense stellar wind near to the star, while the blue shifted absorption lobe is created where the radiation passes through a circumstellar layer of colder material expanding in the direction of the observer. An inverse P Cygni profile is observed in He I line of YSG\_103\_-1, which indicates infalling material towards the central star. Moreover, YSG\_103\_-1 has been characterized as a Be/X-ray pulsar binary system, when it was detected in 2022 as an X-ray transient MAXI J0655-013, as reported in [20] and [16].

Variation in RV The study reflects that this technique can only detect shifts around 0.1 times the resolution, which for R=25000 is equal to 0.019 Å as an average for the three lines. This is equivalent to a shift in velocity space of  $1.12\,\mathrm{km/s}$ . As a result, for shifts lower than the corresponding to  $1.2\,\mathrm{km/s}$ , error exceeds 37%, reaching 100% for values under 0.61 km/s. However, shifts of  $10-100\,\mathrm{km/s}$  are expected for binary systems, but none were detected with the available data.

**Rotation velocity** The results of the four sources'  $v_{rot}\sin i$  are shown in Table II. These values can be compared to the critical rotational velocities of Be stars, taken from [21], for the corresponding stellar

masses. The latter are provided by SHBoost. Upon critical rotation, centrifugal force equals gravitational force, so it defines the threshold where the star begins to lose material. Now,  $v_{rot}$  values are still multiplied by  $\sin i$ ; however, the average value of  $\sin i$  for a uniform distribution of i is 0.62, so if we divide by it, rotation velocities get much close to the critical rotation characteristic of Be stars. The equivalent width values can be found in Appendix B.

Source	Mass	$v_{rot}\sin i$	$v_c$	$v_{rot}\sin i/v_c$
	${\rm M}_{\odot}$	$\mathrm{km/s}$	$\mathrm{km/s}$	
YSG_27_63	5.55	$217\pm7$	429	$0.51 \pm 0.02$
$YSG\_30\_62$	8.57	$222\pm8$	468	$0.47\pm0.02$
YSG_358_63	5.79	$254\pm6$	429	$0.59\pm0.01$
YSG_359_63	5.15	$267\pm19$	418	$0.64 \pm 0.04$

TABLE II:  $v_{rot}\sin i$  computed from He I 4471 Å FWHM.

Other He I lines were taken to compute rotation velocity, but it presented notorious discrepancies, which could arise from underlaying emission that is not directly seen in our data. As an example, the Gaussian fit wasn't successful for the H $\alpha$  line, since the residuals obtained after subtracting the Gaussian model revealed the presence of a faint bi-modal disc emission for this line. The same could be happening to He I emission.

The results show that 21 of the sources CMD were brighter and hotter than the previous data predicted, as can be seen in the CMD in Figure 5, with new positions obtained from two different methods: spectroscopic reddening correction and SHBoost. Extinction estimated from DIBs still yields positions that differ from those derived from SHBoost. This discrepancy may arise from assumptions about the  $R_V$  value, as pointed out in [8]. Therefore, extinction can't be neglected when looking for LRN progenitors in the HG. There was no information of YSG\_104\_-13 in SHBoost, since there wasn't Gaia DR3 XP data. The stellar evolution tracks show that most of our sources, which initially were HG candidates, now have positions more consistent with MS stars of 4-18  $M_{\odot}$ . These stellar tracks are taken from MESA Isochrones and Stellar Tracks (MIST)[9], whose models are computed with the Modules for Experiments in Stellar Astrophysics (MESA)[15] code.

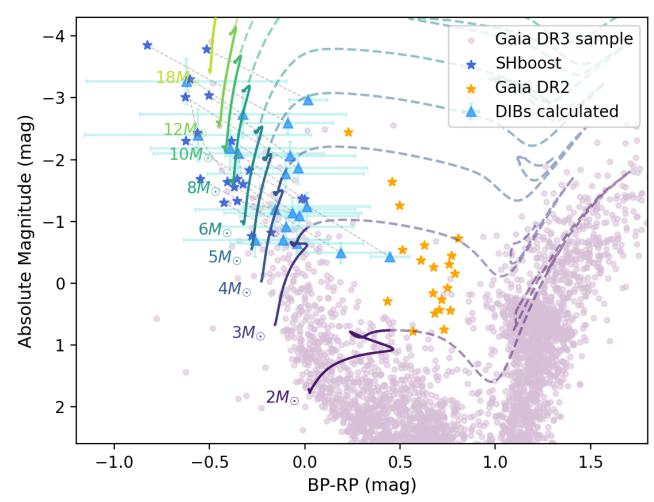


FIG. 5: CMD with Gaia's G-band absolute magnitude versus BP-RP colour, comparing the sources' previous (orange) and actual position (blue and dark blue). A series of discontinuous lines connect the positions of the same source. Lilac-coloured dots represent Gaia DR3 random sample. Evolutionary tracks are shown, spanning from the MS to core helium burning phase for single stars of masses from 2 to  $14M_{\odot}$ , with an initial to critical rotation velocity ratio of 0.4.

#### V. CONCLUSIONS

Upon analysis of the 21 sources data, all were found to be B-type stars, inconsistent with true LRN progenitors' features, which are typically cooler and more evolved systems. This misidentification stems from the effects of interstellar extinction, which reddened the observed photometric data, and would need to be considered in future surveys.

Nevertheless, the selection method proved unexpectedly effective at isolating B-type stars, many of which belongs to the peculiar Be star population. This suggests that it may be a repurposed as a strategy to identify Be stars, even when affected by extinction, offering a pathway for building samples of Be stars for further study.

# ${\bf Acknowledgments}$

I sincerely thank my advisor Nadejda Blagorodnova for her guidance throughout this work. I'm also grateful to my friends and family for their support.

- Addison, H., et al. 2022, MNRAS, 517, 1884
- [2] Bellm, E. C. 2014, The Zwicky Transient Facility
- [3] Blagorodnova, N., et al. 2021, A&A, 653, A134
- [4] Boffin, H. M. J. & Jones, D. 2024
- [5] Brown, A. G. A., et al. 2018, A&A, 616, A1
- [6] Brown, A. G. A., et al. 2021, A&A, 650, C3
- [7] Buil, C. n.d, https://buil.astrosurf.com/us/spe2/hresol7.htm
- [8] Carvalho, A. S. & Hillenbrand, L. A. 2022, AJ, 940, 156
- [9] Choi, J., et al. 2016, Astrophys. J., 823, 102
- [10] Gray, R. O. & Corbally, C. J. 2009 (Princeton U. Press)
- [11] Hanuschik, R. W., et al. 1996, A&AS, 116, 309
- [12] Khalatyan, A., et al. 2024, A&A, 691, A98

- [13] Labadie-Bartz, J., et al. 2018, AJ, 155, 53
- [14] Otero, S. 2011, Delta Scorpii: the Birth of a Be Star, https://www.aavso.org/vsots\_delsco
- [15] Paxton, B., et al. 2011, ApJS, 192, 3
- [16] Reig, P., et al. 2022, ATel, 15612, 1
- [17] Rivinius, T., et al. 2013, A&AR, 21, 69
- [18] Rodrigo, C. & Solano, E. 2020, 182
- [19] Sana, H., et al. 2012, Science, 337, 444–446
- [20] Serino, M., et al. 2022, ATel, 15442, 1
- [21] Townsend, R. H. D., et al. 2004, MNRAS, 350, 189–195
- [22] Tylenda, R., et al. 2011, A&A, 528, A114
- [23] Vallenari, A., et al. 2023, A&A, 674, A1

# Caracterització de candidats a progenitors de fusions estel·lars

Author: Hui Hui Zhang Guo, hzhanggu<br/>7@alumnes.ub.edu<br/> Facultat de Física, Universitat de Barcelona, Diagonal 645, 08028 Barcelona, Spain.

Advisor: Nadejda Blagorodnova, nblago@fqa.ub.edu

Resum: Tradicionalment, les fusions estel·lars s'han detectat a través de les seves explosions. Un estudi previ de Addison et al. (2022) va proposar un mètode per seleccionar-los en funció de la seva posició en el Hertzsprung Gap i un augment de la lluminositat, encara que sense valors d'extinció, donant lloc a 21 candidats a progenitors de Luminous Red Novae (LRNe). Presentem la seva caracterització basada en noves dades fotomètriques i espectroscòpiques. Inicialment identificats com a estrelles grogues, tots els candidats van ser reclassificats com a estrelles calentes de tipus B, la majoria d'elles com a estrelles Be, cosa que fa poc probable que siguin genuïnament progenitors de LRNe. Aquests resultats destaquen la necessitat d'incorporar correccions d'extinció per evitar la caracterització errònia a causa dels efectes d'envermelliment. També calculem la variació en les velocitats radials per tal de decidir si poden ser sistemes binaris i velocitats de rotació per a les fonts sense línies d'emissió, ja que les estrelles Be tenen alta velocitat de rotació. Com és d'esperar, el ratio entre la seva velocitat de rotació (multiplicada per sini) i la velocitat crítica és de 0, 47-0, 64. Paraules clau: Astrofísica, Astronomia Observacional, Transicions Atòmiques.

ODSs: Educació de qualitat, Igualtat de gènere.

### Objectius de Desenvolupament Sostenible (ODSs o SDGs)

1. Fi de la es desigualtats		10. Reducció de les desigualtats
2. Fam zero		11. Ciutats i comunitats sostenibles
3. Salut i benestar		12. Consum i producció responsables
4. Educació de qualitat	Х	13. Acció climàtica
5. Igualtat de gènere	X	14. Vida submarina
6. Aigua neta i sanejament		15. Vida terrestre
7. Energia neta i sostenible		16. Pau, justícia i institucions sòlides
8. Treball digne i creixement econòmic		17. Aliança pels objectius
9. Indústria, innovació, infraestructures		

El contingut d'aquest TFG part d'un grau universitari de Física, i es relaciona amb l'ODS 4, ja que contribueix a l'educació a nivell universitari. En particular, la recerca astronòmica avançada, com la que es descriu, fomenta la formació de científics altament qualificats. Promoure aquest tipus d'estudis a les universitats i centres educatius és clau per a millorar la qualitat educativa. També es pot relacionar amb l'ODS 5, ja que aquest treball, realitzat i supervisat per dues dones, exemplifica la importància de promoure la presència i el reconeixement de les dones en l'àmbit científic, contribuint a trencar estereotips i fomentar la igualtat de gènere en les disciplines STEM."

Treball de Fi de Grau 6 Barcelona, Juny 2025

# Appendix A: LIGHT-CURVE DATA

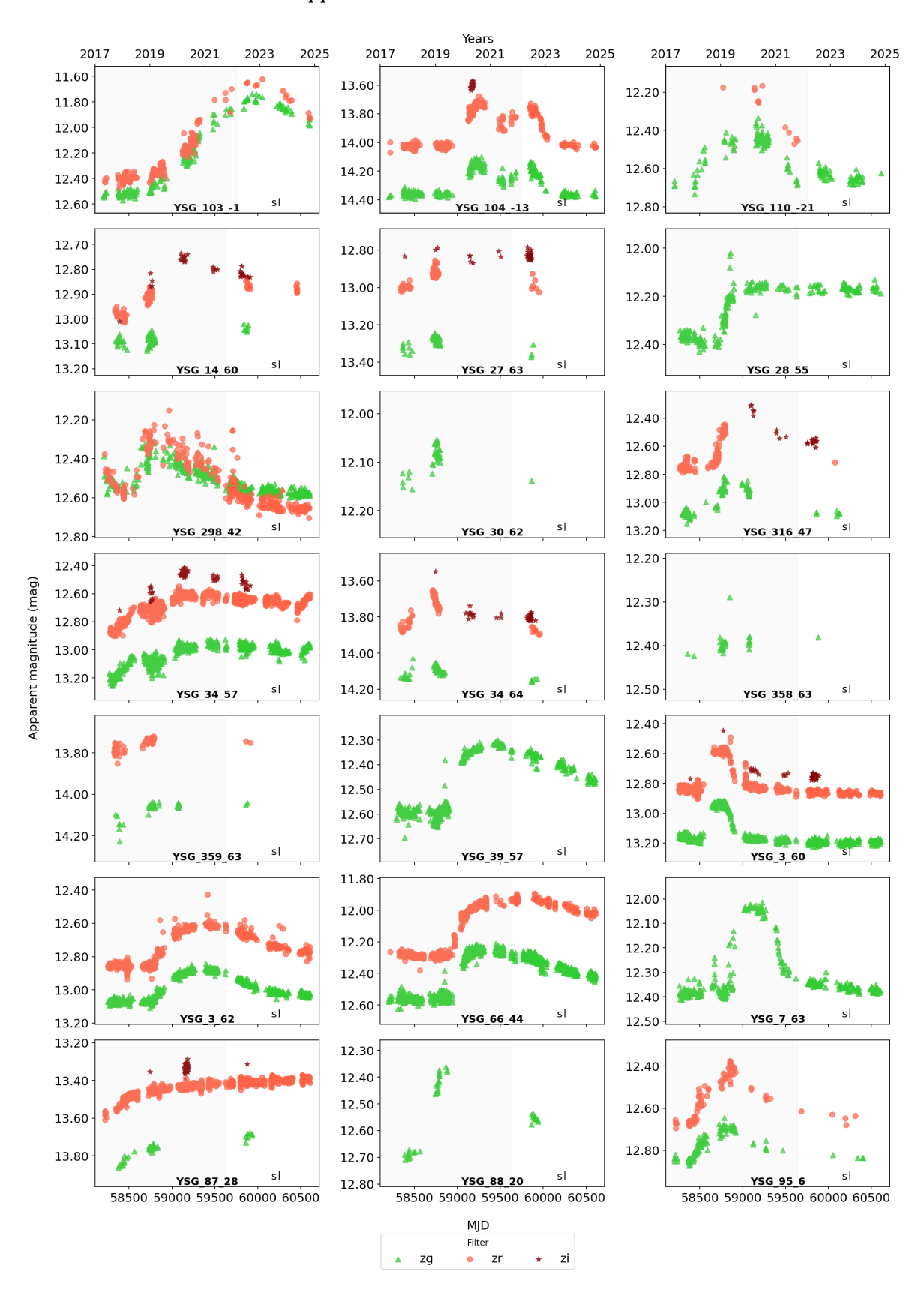


FIG. 6: Light-curves of the LRN candidates shown as apparent magnitude versus time in MJD and years in different filters, taken from ZTF. A grey background shows the available information that the original article had access to (February 2022).

# Appendix B: SPECTROSCOPIC DATA

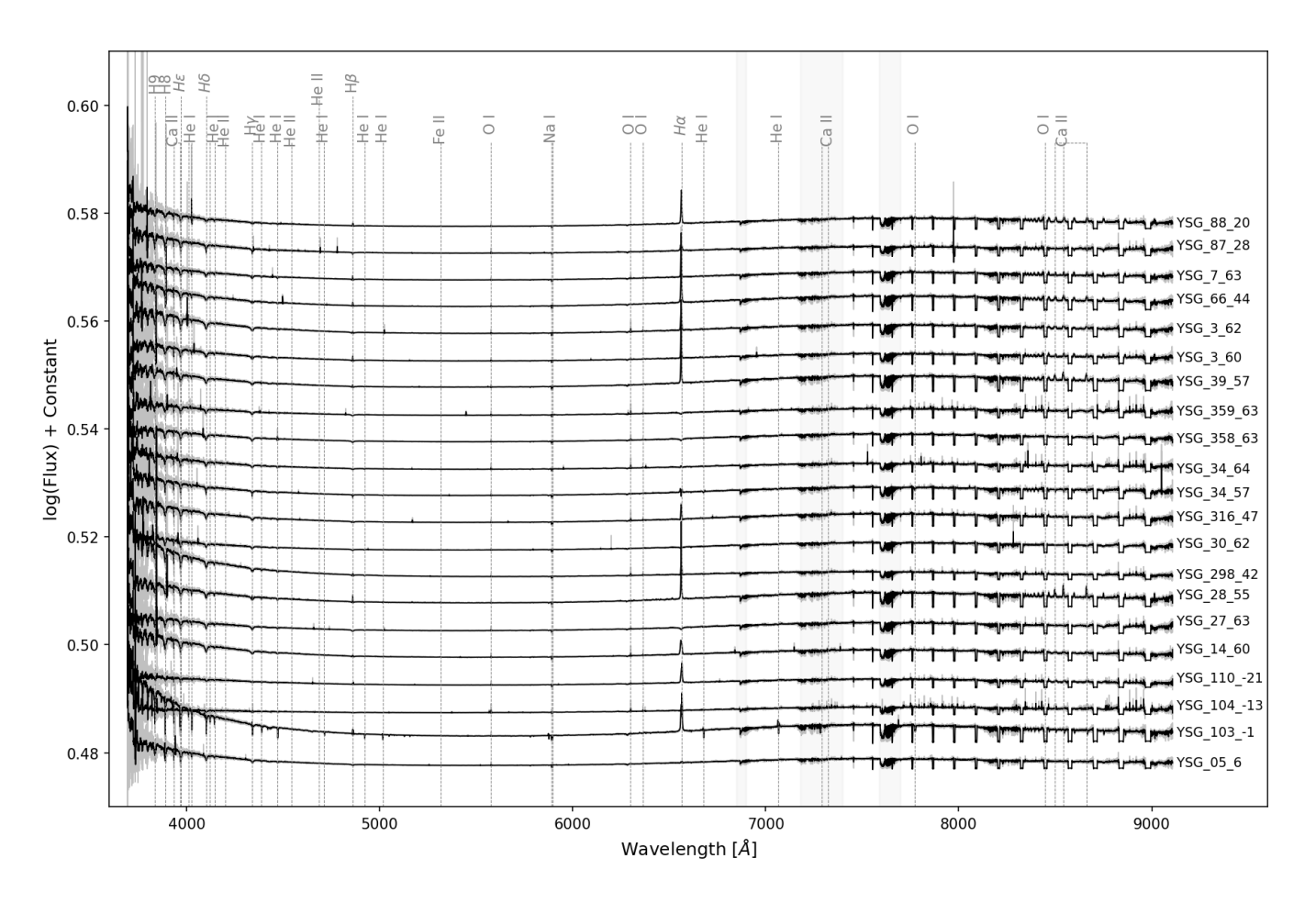


FIG. 7: Spectrum of the 21 sources as natural logarithm of flux plus constant versus wavelength. Most important emission and absorption lines are indicated, as well as telluric absorption. The grey spectrum shows original spectrum without smoothing process for display purposes.

Source	Equivalent Width	Source	Equivalent Width
	Å		Å
YSG_1031	0.228	YSG_358_63	0.170
YSG_10413	0.223	YSG_359_63	0.177
YSG_11021	0.126	YSG_39_57	0.203
$YSG_14_60$	0.127	YSG_3_60	0.155
$YSG_27_63$	0.174	YSG_3_62	0.183
$YSG_28_55$	0.065	YSG_66_44	0.155
$YSG\_298\_42$	0.014	YSG_7_63	0.174
$YSG\_30\_62$	0.271	YSG_87_28	0.310
YSG_316_47	0.052	YSG_88_20	0.171
$YSG_34_57$	0.203	YSG_95_6	0.264
YSG_34_64	0.215		

TABLE III: Equivalent width values for the 21 sources.

Treball de Fi de Grau 8 Barcelona, Juny 2025

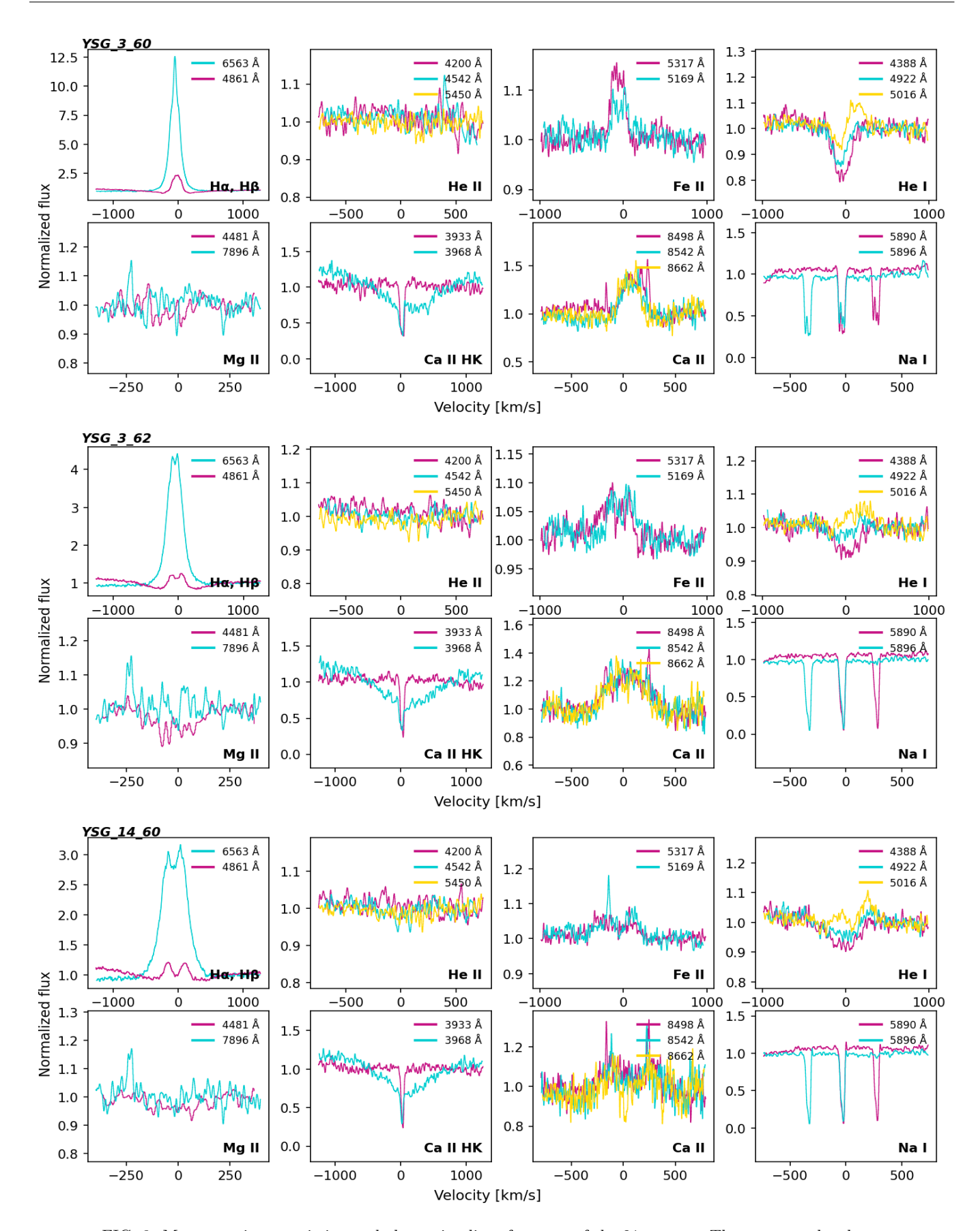


FIG. 8: Most prominent emission and absorption lines for some of the 21 sources. The spectrum has been continuum-normalized dividing the flux by the mean level computed from regions adjacent to the line, excluding the line core.

Treball de Fi de Grau 9 Barcelona, Juny 2025

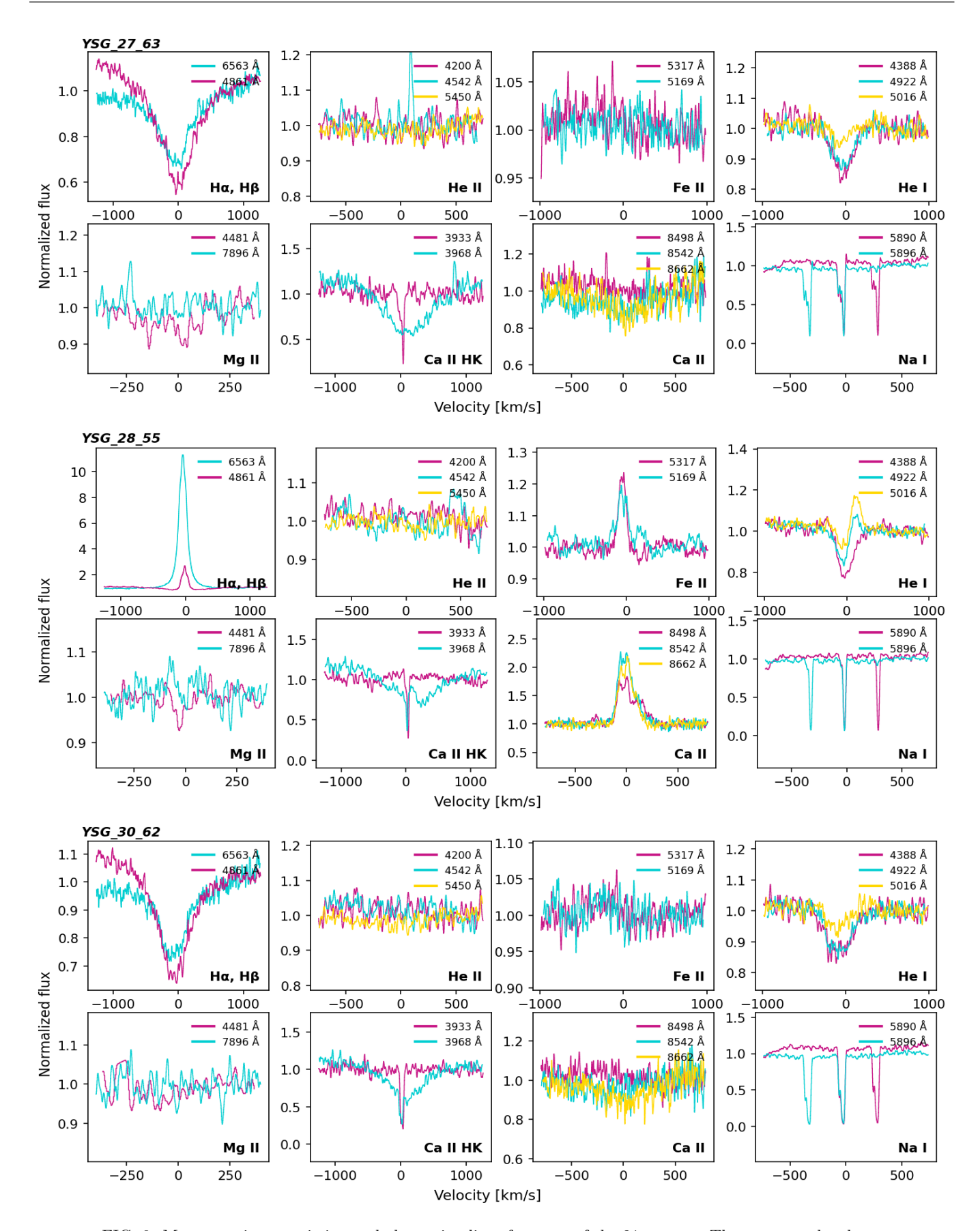


FIG. 9: Most prominent emission and absorption lines for some of the 21 sources. The spectrum has been continuum-normalized dividing the flux by the mean level computed from regions adjacent to the line, excluding the line core.

Treball de Fi de Grau 10 Barcelona, Juny 2025

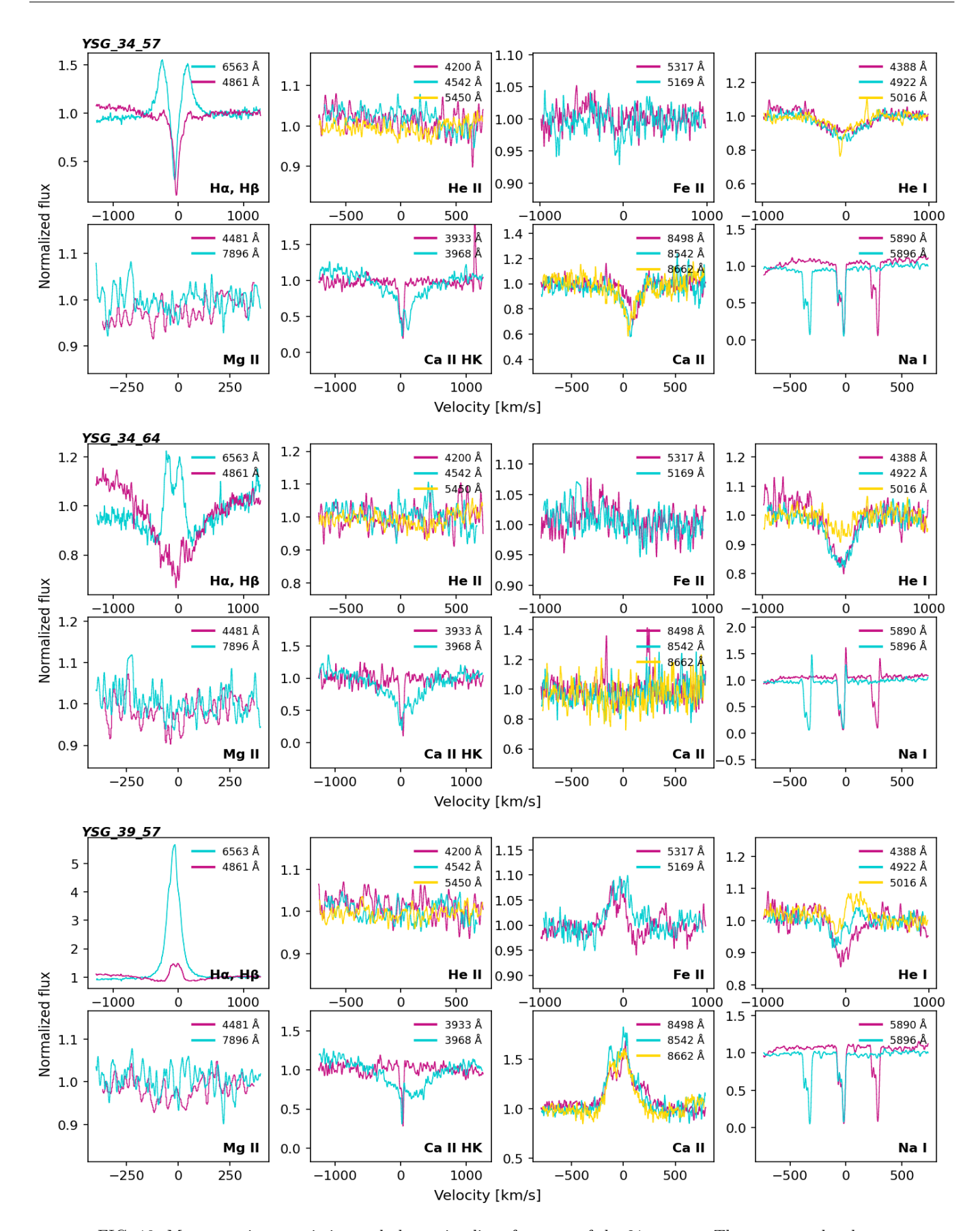


FIG. 10: Most prominent emission and absorption lines for some of the 21 sources. The spectrum has been continuum-normalized dividing the flux by the mean level computed from regions adjacent to the line, excluding the line core.

Treball de Fi de Grau 11 Barcelona, Juny 2025

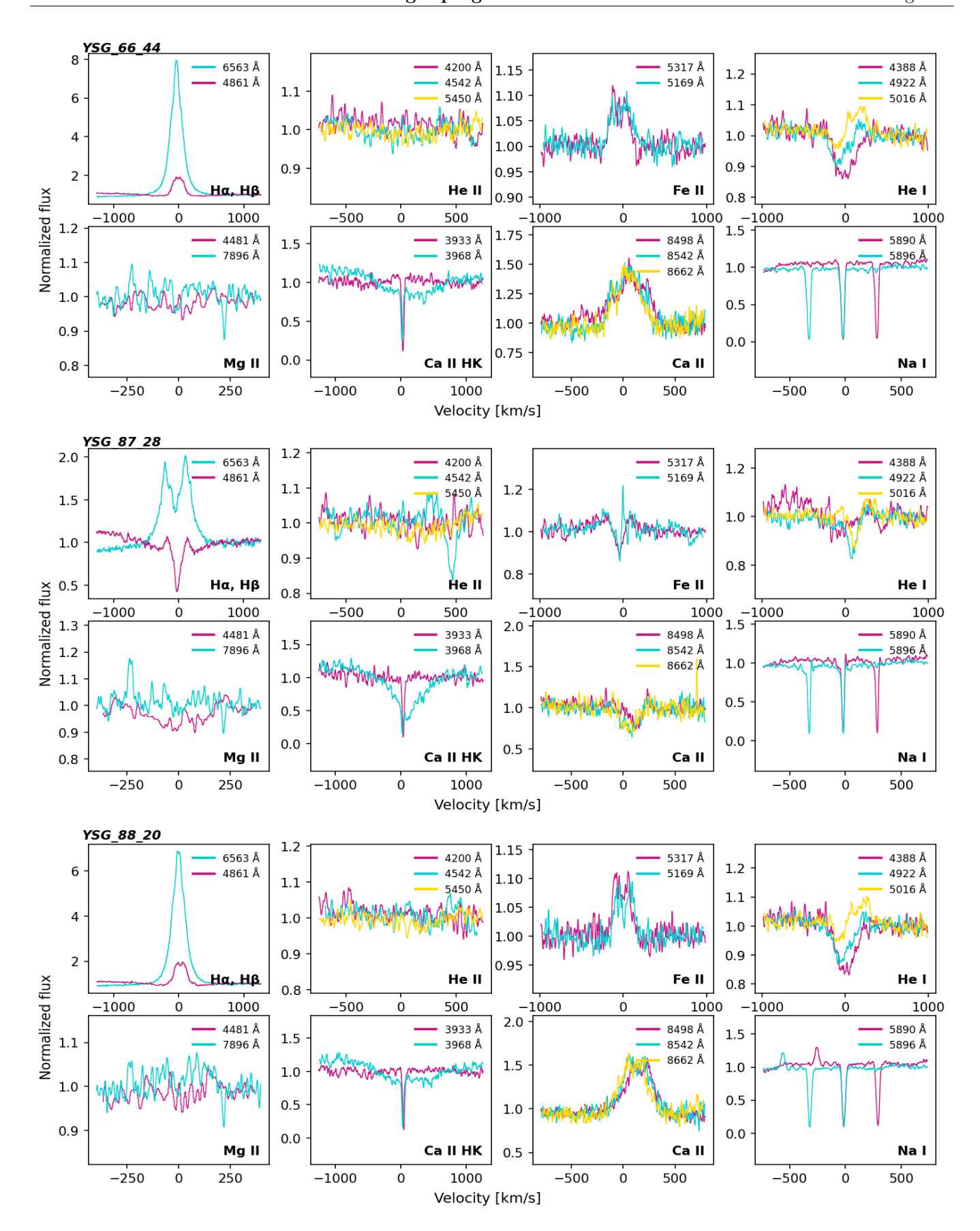


FIG. 11: Most prominent emission and absorption lines for some of the 21 sources. The spectrum has been continuum-normalized dividing the flux by the mean level computed from regions adjacent to the line, excluding the line core.

Treball de Fi de Grau 12 Barcelona, Juny 2025

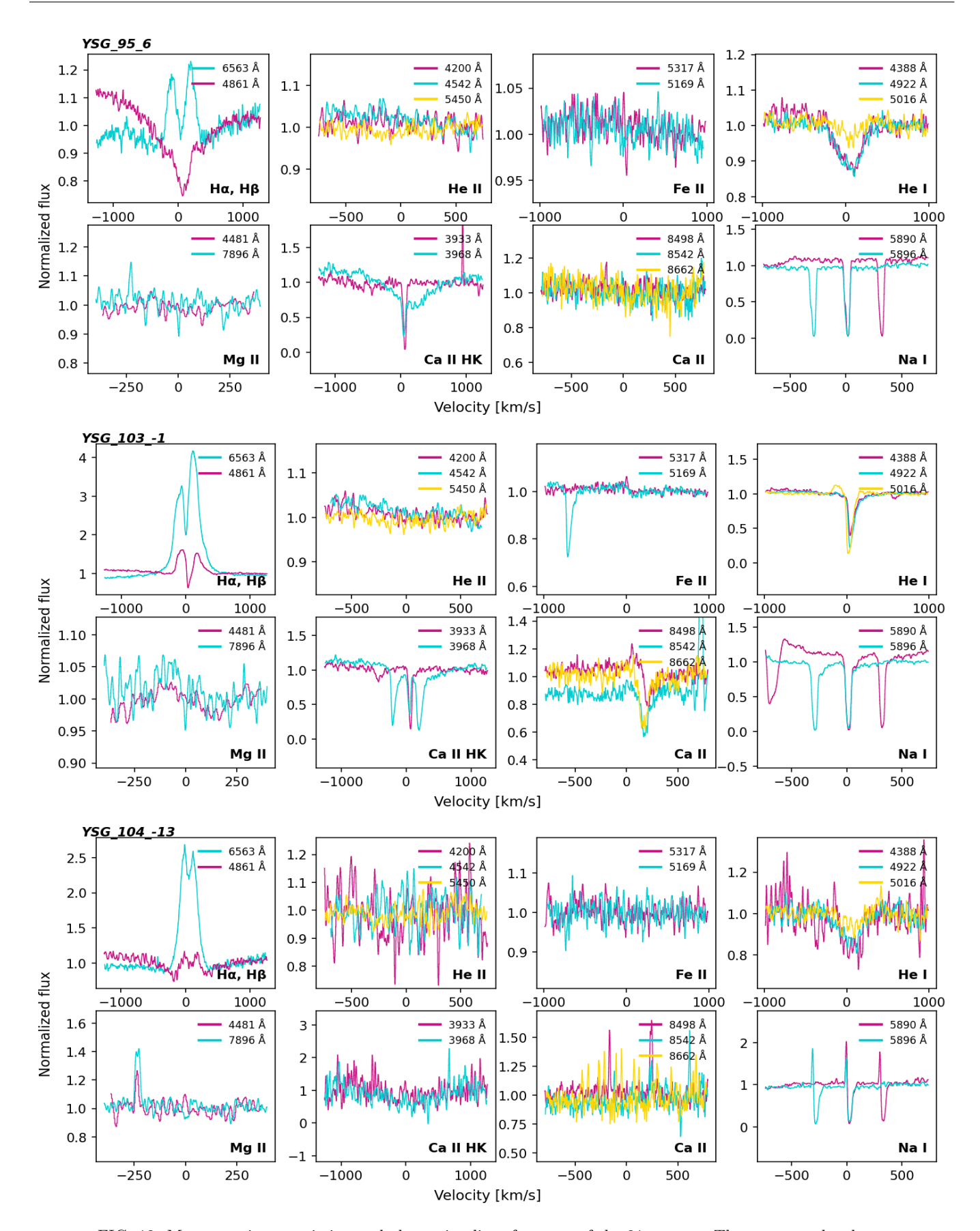


FIG. 12: Most prominent emission and absorption lines for some of the 21 sources. The spectrum has been continuum-normalized dividing the flux by the mean level computed from regions adjacent to the line, excluding the line core.

Treball de Fi de Grau 13 Barcelona, Juny 2025

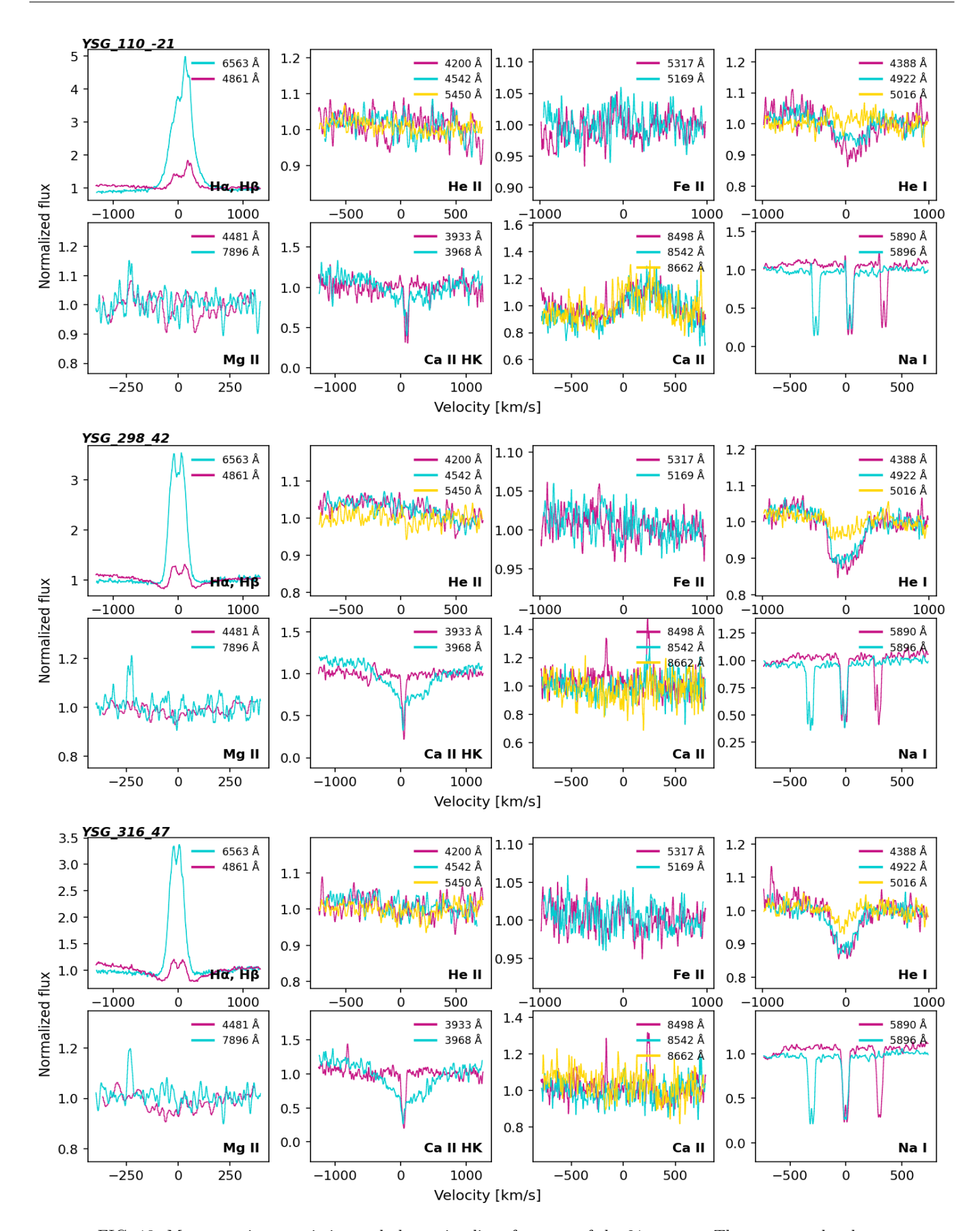


FIG. 13: Most prominent emission and absorption lines for some of the 21 sources. The spectrum has been continuum-normalized dividing the flux by the mean level computed from regions adjacent to the line, excluding the line core.

Treball de Fi de Grau 14 Barcelona, Juny 2025

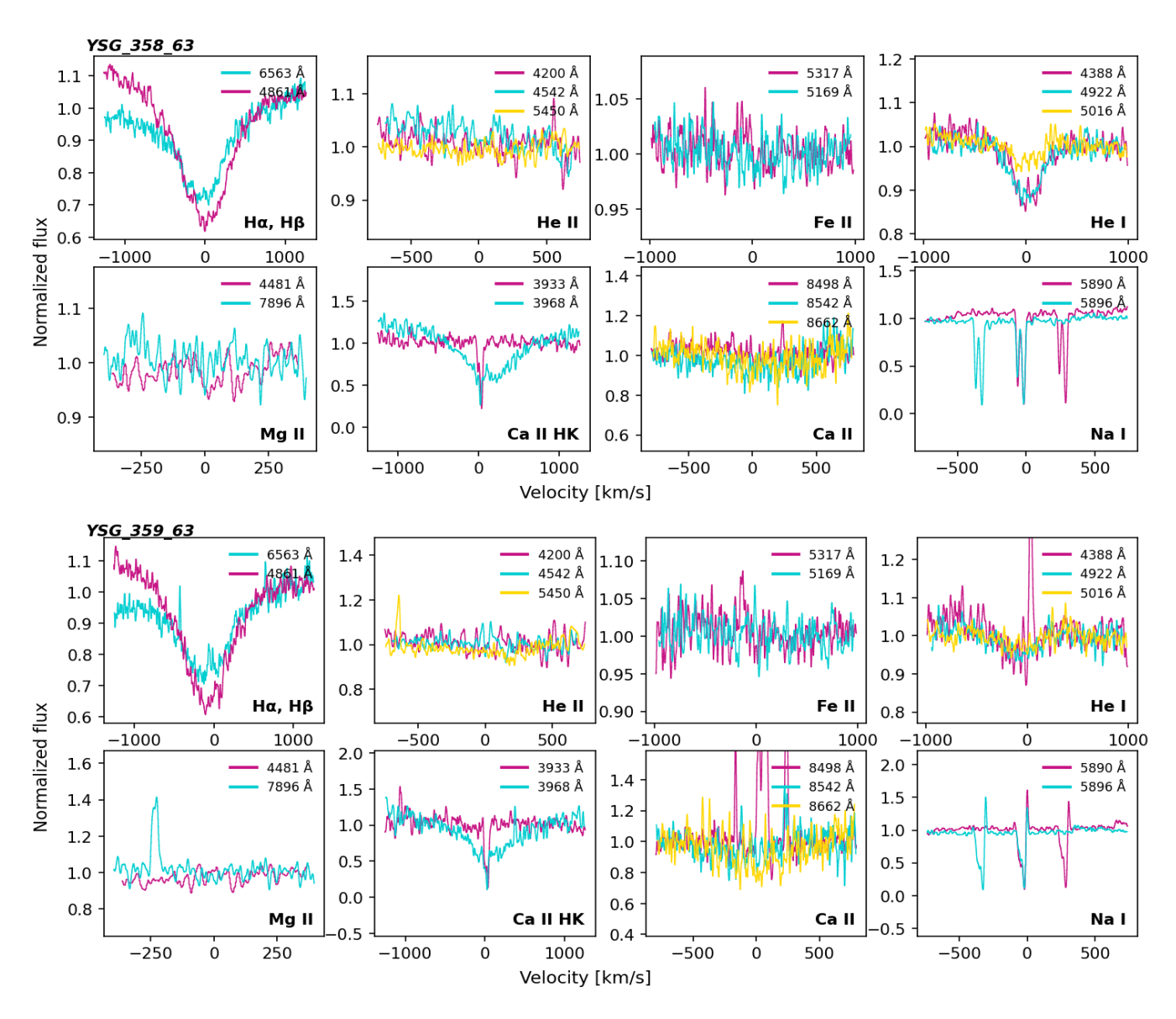


FIG. 14: Most prominent emission and absorption lines for some of the 21 sources. The spectrum has been continuum-normalized dividing the flux by the mean level computed from regions adjacent to the line, excluding the line core.

Treball de Fi de Grau 15 Barcelona, Juny 2025